Spontaneous Bulk-surface Charge Separation of TiO_2-{001} Nanocrystals Leads to High Activity in Photocatalytic Methane Combustion

Cong Fu,[a‡] Fei Li,[b‡] Jianlong Yang, [c‡] Jijia Xie,[d] Yunshang Zhang,[a] Xiao Sun, [a] Xusheng Zheng,[e] Yuanxu Liu,[a,f] Junfa Zhu,[e] Junwang Tang, [d]* Xue-Qing Gong [b]* and Weixin Huang [a,g]*

[a] Hefei National Laboratory for Physical Sciences at the Microscale, Key Laboratory of Surface and Interface Chemistry and Energy Catalysis of Anhui Higher Education Institutes, and Department of Chemical Physics, University of Science and Technology of China, Hefei 230026, P. R. China

[b] Key Laboratory for Advanced Materials, Centre for Computational Chemistry and Research Institute of Industrial Catalysis, School of Chemistry and Molecular Engineering, East China University of Science and Technology, Shanghai 200237, P. R. China

[c] Key Lab of Synthetic and Natural Functional Molecule Chemistry of Ministry of Education, the Energy and Catalysis Hub, College of Chemistry and Materials Science, Northwest University, Xi'an 710127, P. R. China

[d] Department of Chemical Engineering, University College London, Torrington Place, London WC1E 7JE, UK

[e] National Synchrotron Radiation Laboratory, University of Science and Technology of China, Hefei 230026, P. R. China

[f] School of Pharmacy, Anhui University of Chinese Medicine, Anhui Academy of Chinese Medicine, Hefei 230012, P. R. China

[g] Dalian National Laboratory for Clean Energy, Chinese Academy of Sciences, Dalian 116023, P. R. China

ABSTRACT: Photocatalytic methane combustion is a promising strategy to eliminate methane at ambient condition, but efficient photocatalysts still lack. Herein, we report that uniform anatase TiO_2 nanocrystals predominantly enclosed with the {001} facets exhibit high activity in photocatalytic catalyzing methane combustion at RT in a flow-bed reactor. The photocatalytic methane reaction rate is 17.6 $mmol_{CH4}{\cdot}h^{-1}{\cdot}g_{catalyst}^{-1}$, which is about 6 and 7 times of those catalyzed by TiO_2 nanocrystals predominantly enclosed with the {100} facets or with the {101} facets. The valence band maximum and conduction band minimum were found to locate space-separately for TiO_2-{001} nanocrystals terminated with the reconstructed (001)-(1×4) surface, at the surface and in the bulk, respectively. Meanwhile, the HOMO of methane adsorbed at the fourfold-coordinated Ti_{4c} site of reconstructed TiO_2(001)-(1×4) surface is located at the valence band maximum of TiO_2, respectively. Upon UV light illumination, TiO_2-{001} nanocrystals exhibit spontaneous bulk-surface charge separation of photo-excited holes and electrons, leading to large concentrations of photoexcited holes on the surface, and subsequent facile interfacial hole transfer from TiO_2(001) surface to adsorbed methane, leading to efficient methane combustion reaction.

KEYWORDS. Photocatalysis, surface photochemistry, reaction mechanism, charge transfer, electronic structure

Methane (CH_4) is the largest constituent of natural gas and widely used in power and heat generations,[1-3] during which unburned CH_4 is unavoidable in exhaust streams. CH_4 is a greenhouse gas with an effect nearly 30 times higher than that of CO_2,[4,5] thus unburned CH_4 in exhaust streams needs to be eliminated prior to emissions. Thermocatalytic combustion using supported precious metal catalysts or transition metal oxide catalysts is the common strategy to eliminate CH_4, but it generally operates high reaction temperatures due to the high stability of CH_4[6-8] and simultaneously produces toxic nitrogen oxides. Photocatalysis utilizing sustainable solar energy has been demonstrated capable of driving CH_4 combustion at ambient condition,[9,10] but efficient photocatalysts lack.

Titanium dioxide (TiO_2) is the most widely used photocatalyst in environmental and energy photocatalysis.[11-12] Using uniform TiO_2 nanocrystals (NCs) with various morphologies and consequently exposed facets, the facet-dependent photocatalytic activity of TiO_2 have been extensively demonstrated.[13-14] Particularly of interest is the anatase TiO_2 {001} facets which are predicted as the active facets for photocatalytic reactions.[15-16] It was reported that anatase TiO_2 NCs with predominantly-exposed {001} facets (denoted as TiO_2-{001}) exhibited superior photocatalytic activity,[17-22] but arguments exist.[23-25] Experimental evidence were observed that, upon photoexcitation, the TiO_2 {001} facets are enriched with photo-excited holes and act as the oxidation sites while the TiO_2{101} facets are enriched with photo-excited electrons and act as the reductive sites.[26-29] The surface structure-dependent surface sites and resulting surface species were also reported to affect the photocatalytic activity of TiO_2.[14,30-31] TiO_2 was studied as photocatalysts for photocatalytic combustion of methane.[32] Meanwhile, Ag-loaded TiO_2 NCs photocatalysts were reported to exhibit facet dependent performance in photocatalytic methane oxidation to liquid-phase oxygenates under a aqueous-phase reaction condition of 2 MPa CH_4 and 0.1 MPa O_2.[33] In this letter, we report strong facet effect of anatase TiO_2 NCs on the photocatalytic activity toward methane combustion under a flow reaction condition of 0.15 atm CH_4 and 0.05 atm O_2 balanced with N_2. TiO_2-{001} NCs was found to exhibit a high photocatalytic CH_4 combustion rate of 17.6 $mmol_{CH4}{\cdot}h^{-1}{\cdot}g_{catalyst}^{-1}$ measured in a flow-bed reactor mode, much higher than those catalyzed by TiO_2 nanocrystals predominantly enclosed with the {100} facets (denoted as TiO_2-{100}) or with the {101} facets (denoted as TiO_2-{101}). Combined experimental characterization and theoretical calculation results demonstrate the unique roles of reconstructed (001)-(1×4) surface with fourfold-coordinated Ti_{4c} sites of TiO_2-{001} NCs in inducing spontaneous bulk-surface charge separation of photo-excited holes and electrons and mediating efficient

interfacial hole transfer from (001)-(1×4) surface to CH_4 adsorbed at the Ti_{4c} sites, both of which lead to the exceptionally high photocatalytic activity.

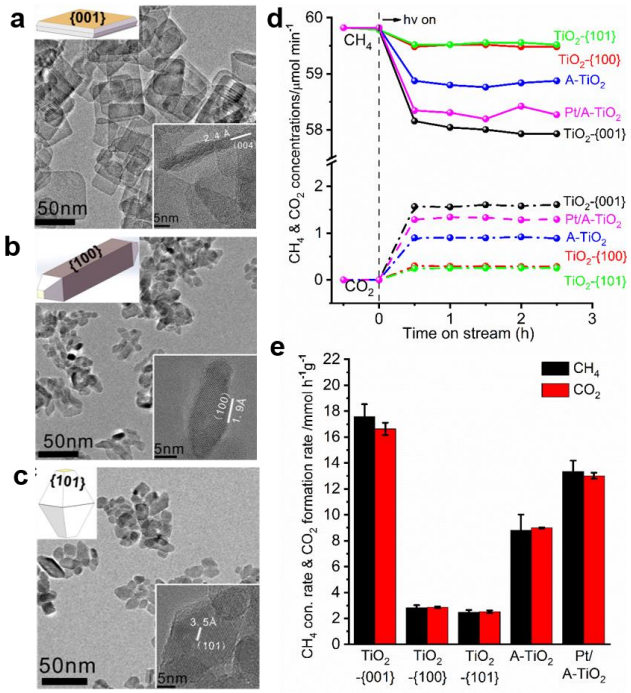

Figure 1. Representative TEM images with inserted HRTEM images and morphology illustrations of (**a**) TiO_2 -{001}, (**b**) TiO_2 -{100}, and (**c**) TiO_2 -{101} NCs. (**d**) CH_4 and CO_2 concentrations as a function of time on stream measured during photocatalytic methane combustion over various TiO_2 NCs and referring commercial anatase TiO_2 and Pt/ TiO_2 photocatalysts in a flow-bed mode (catalyst amount: 6 mg; reactant: CH_4:O_2=15%:5% balanced with N_2 at a flow rate of 9 mL·min^{-1}; temperature: 45 °C; light: 70 W LED at 365 nm). (**e**) Photocatalytic CH_4 conversion and CO_2 formation rates over various TiO_2 NCs, commercial anatase TiO_2 and Pt/ TiO_2 photocatalysts.

Uniform anatase TiO_2-{001}, TiO_2-{100} and TiO_2-{101} NCs were synthesized following previous recipes[34] and characterized microscopically and spectroscopically (Figure 1a-c and Figure S1-S3). All samples exhibit a pure anatase phase, uniform morphologies, similar average sizes of around 12 nm, and similar specific surface areas of around 100 m^2/g. The percentages of {001} facets in TiO_2-{001}, {100} facets in TiO_2-{100}, and {101} facets in TiO_2-{101} NCs were estimated to be around 80% [34]. XPS results observed carbonates, hydroxyl and water on the surfaces of all TiO_2 NCs, resulting from ambient CO_2 and H_2O adsorption, but few anions (F^-, SO_4^{2-} and Cl^-) used during the synthesis. A reference sample, Pt/A-TiO_2 with a Pt loading of 1.24 wt.%, was prepared on commercial anatase TiO_2 (A-TiO_2) (Aladdin) using photodeposition method (Figure S4).[35]

Photocatalytic performance in CH_4 combustion was evaluated using a customer-designed flow-bed reactor (Figure S5)[35] under a 365 nm LED light illumination at RT. The actual temperature of illuminated photocatalysts was measured as 45 °C. Only CO_2 was detected as the product (Figure S6). Figure 1d shows variations of measured CH_4 and CO_2 concentrations as a function of reaction time during photocatalytic CH_4 combustion catalyzed by various TiO_2 NCs and reference samples A-TiO_2 and Pt/A-TiO_2 (catalyst amount: 6 mg). Upon the LED light illumination, the CH_4 concentration decreases, accompanied by the emergence of CO_2. All photocatalysts are stable within 3 h. The photocatalytic performance of each catalyst at the reaction time of 30 min was evaluated four times to give reliable photocatalytic CH_4 conversion rate and CO_2 formation rate (Figure 1e), which are almost same. After the LED light is turned off, CH_4 resumes the original concentration and CO_2 disappears (Figure S7). All these observations confirm the occurrence of photocatalytic CH_4 combustion under the employed reaction condition. Clearly, various TiO_2 NCs exhibit facet-dependent photocatalytic performance. TiO_2-{001} NCs are most active. Upon the LED light illumination, the CH_4 concentration decreases from 59.8 μ mol_{CH4}·min^{-1} to around 58.0 μmol_{CH4}·min^{-1} for TiO_2-{001} NCs and the produced CO_2 concentration is around 1.6 μ mol_{CO2}·min^{-1}. The calculated mass-specific CH_4 conversion rate of TiO_2-{001} NCs is 17.6 $mmol_{CH4}$·h^{-1}·$g_{catalyst}^{-1}$, almost 6 and 7 times of those of TiO_2-{100} (2.8 $mmol_{CH4}$·h^{-1}·$g_{catalyst}^{-1}$) and TiO_2-{101} (2.5 $mmol_{CH4}$·h^{-1}·$g_{catalyst}^{-1}$) NCs. Commercial A-TiO_2 exhibits a mass-specific CH_4 conversion rate of 8.8 $mmol_{CH4}$·h^{-1}·$g_{catalyst}^{-1}$, and Pt/A-TiO_2 exhibits a higher mass-specific CH_4 conversion rate of 13.3 $mmol_{CH4}$·h^{-1}·$g_{catalyst}^{-1}$ due to the co-catalyst effect of Pt. It can be seen that TiO_2-{001} NCs is even more photocatalytic active than 1.24 wt.%-Pt/A-TiO_2 photocatalyst, which is unusual because Pt is well-known to be an excellent co-catalyst for TiO_2 photocatalysts. Photocatalytic performance of TiO_2-{001} NCs and Pt/A-TiO_2 films prepared with different amounts of photocatalysts and consequently different thicknesses of films was evaluated (Figure S8), in which with the same photocatalyst amount, TiO_2-{001} NCs films are always more photocatalytic active than Pt/A-TiO_2 films. The apparent quantum efficiency of TiO_2{001} NCs in photocatalytic CH_4 combustion irradiated with the LED light at 365 nm was measured as around 0.1%. The CH_4 conversion increases slowly with the used photocatalyst amount increasing from 6 mg to 50 mg, while the mass-specified CH_4 conversion rate keeps decreasing. This can be mainly attributed to the fact that the photo absorption of photocatalysts in the film weakens with the distance of the photocatalysts to the film surface increasing. Photocatalytic performance of TiO_2-{001} NCs and Pt/A-TiO_2 was further evaluated under the reactants with different CH_4:O_2 ratios (Figure S9), in which TiO_2-{001} NCs are always more photocatalytic active than Pt/A-TiO_2. There is an optimal reactant composition for photocatalytic CH_4 combustion, which is an interesting issue deserving further studies. These photocatalytic reaction results demonstrate TiO_2-{001} NCs as a highly active photocatalyst for methane combustion at RT, which is also supported by comparisons with previously-reported photocatalysts for methane combustion (Table S1)[36-40].

Various TiO_2 NCs exhibit almost identical UV-Vis diffuse reflectance spectra and similar valence band photoelectron spectra (Figure S10 a and b), indicating that they should exhibit similar light absorption and charge generation processes. TiO_2-{001} NCs exhibit much higher concentrations of paramagnetic species formed by trapped photoexcited charges, such as Ti^{3+}, O_2^- and O^- under UV light illumination than TiO_2-{101} and TiO_2-{100} NCs (Figure S10c) and consequently a stronger PL intensity (Figure S10d). Photoexcited free electrons in the conduction band of TiO_2 was reported to exhibit a broad IR absorption feature starting at ~4000 cm^{-1} and increasing exponentially up to 1700 cm^{-1}.[41] Temporal evolutions were monitored using in situ DRIFTS spectra (Figure S11). Using the absorbance at 2000 cm^{-1} as the representative, the density of photoexcited electrons in the conduction band of all TiO_2 NCs initially grows due to the dominant charge generation and separation processes and then decays gradually to almost the background due to the dominant charge recombination processes (Figure 2a). The maximum density of photoexcited

electrons in the conduction band of TiO_2-{001} NCs is significantly higher than of TiO_2-{101} and TiO_2-{100} NCs, while the decay rate is much smaller. Thus, TiO_2-{001} NCs exhibit greatly higher densities and longer life of both trapped and free photoexcited charges than TiO_2-{101} and TiO_2-{100} NCs upon UV light illumination, demonstrating much more efficient charge separation processes.

Above PL, ESR and IR results are mainly related to the photoexcited charges in the bulk of various TiO_2 NCs, which need to migrate to the surface to participate surface reactions. NEXAFS spectra in the mode of total electron yield are powerful in probing electronic structures of solid surfaces. As schematically illustrated in Figure 2b, the O K-edge NEXAFS feature of TiO_2 probes the electron transition from the occupied O 1*s* orbital to the O 2*p* orbital, whose probability is proportional to the density of unoccupied O 2*p* states, while the Ti L-edge NEXAFS feature of TiO_2 probes the electron transition from the occupied Ti 2*p* orbital to the Ti 3*d* orbital, whose probability is proportional to the density of unoccupied Ti 3*d* states. UV light illumination on TiO_2 excites the electron transition from the valence band consisting of the O 2*p* orbital to the conduction band consisting of Ti 3*d* orbital, increasing the density of unoccupied O 2*p* states but decreasing the density of unoccupied Ti 3*d* states, respectively. Consequently, the O K-edge NEXAFS features of various TiO_2 NCs grow upon UV light illumination whereas the corresponding Ti L-edge NEXAFS features weaken (Figure 2c and Figure S12). In the O K-edge NEXAFS spectra, the features f and g arise from the O 2*p* states hybridized with the Ti 3*d* states and the features h, i and j are ascribed to the O 2*p* antibonding state hybridized with the Ti 4*s* and 4*p* states, while in the Ti L-edge NEXAFS spectra, the feature a is related to dipole-forbidden transitions induced by multiple interaction and the features b/c1/c2 and d/e correspond to the L_3-edge ($2p_{3/2}\rightarrow 3d$) and L_2-edge ($2p_{1/2}\rightarrow 3d$) transitions, respectively.[42] Principally, the gain of the O K-edge NEXAFS features ($\Delta I_{O\ K\text{-}edge}$) and the loss of the Ti L-edge NEXAFS features ($\Delta I_{Ti\ L\text{-}edge}$) of TiO_2 upon UV light illumination should be same when the charge generation, separation and recombination processes all occur locally at the surface, however, the observed $\Delta I_{OK\text{-}edge}/\Delta I_{Ti\ L\text{-}edge}$ ratio varies with the facets exposed on TiO_2 NCs (Figure 2d), being 2.08, 1.25 and 0.89 for TiO_2-{001}, TiO_2-{101} and TiO_2-{100} NCs, respectively. Such deviations can be rationalized by the occurrence of bulk-surface charge separation within TiO_2 NCs. Therefore, under UV light illumination, the bulk↔surface charge separation within TiO_2-{001} NCs is much more efficient than within TiO_2-{101} and TiO_2-{100} NCs; moreover, the bulk→surface migration of holes and the surface→bulk migration of electrons should occur for TiO_2-{001} NCs, leading to the most efficient charge separation process and strongly photoexcited holes-enriched surface for TiO_2-{001} NCs. These results for the first time explore NEXAFS as a powerful technique for characterizing the bulk-surface charge separation processes of semiconductors upon photoexcitation. Meanwhile, tiny Ti^{3+} features at ~0.7 eV below the Fermi level[43] were observed in valence-band photoemission spectra of various TiO_2 NCs under UV light illumination (Figure S13), suggesting the reduction of Ti^{4+} by photoexcited electrons.

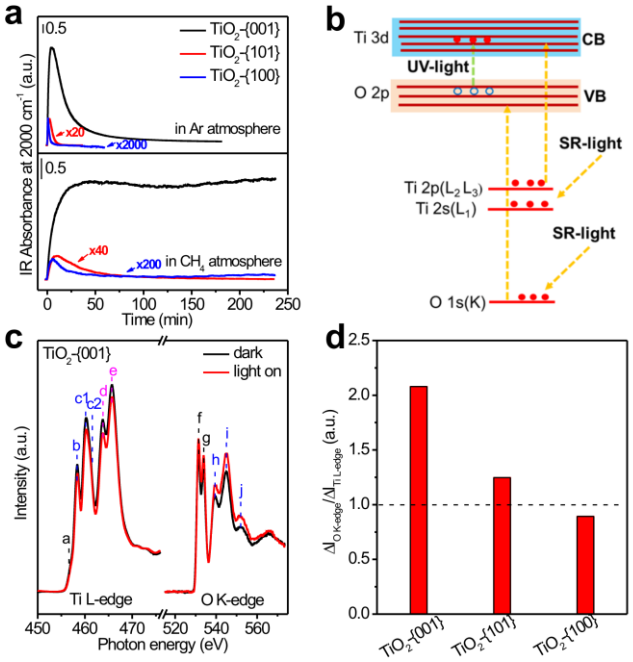

Figure 2. (**a**) Temporal evolutions of the IR absorbance intensity at 2000 cm^{-1} of various TiO_2 NCs upon UV light illumination at 298 K in Ar and CH_4 atmosphere. (**b**) Schematic illustration of NEXAFS working principle of TiO_2 upon UV light illumination. (**c**) Ti L-edge and O K-edge NEXAFS spectra of TiO_2-{001} NCs in the dark and under light irradiation. (**d**) $\Delta I_{O\ K-edge}/\Delta I_{Ti\ L-edge}$ values of various TiO_2 NCs induced by UV light illumination.

Photoexcited charges on TiO_2 surface undergo the interfacial charge transfer to adsorbed molecules to drive photocatalytic reactions. O_2 adsorption on various TiO_2 NCs was reported similar[30] and adsorbed O_2 can facilely trap photoexcited electrons on TiO_2 surfaces.[44] DRIFTS spectra of various TiO_2 NCs in CH_4 atmosphere under dark condition and followed by Ar purging at RT (Figure S14) exclude the irreversible adsorption of CH_4 on various TiO_2 NCs at RT, whereas adsorption-microcalorimetry measurements (Figure S15) demonstrate reversible adsorption of CH_4 with calculated adsorption amount and integral adsorption heat as 0.93 μmol/m^2 and 18.5 kJ/mol, 1.6 μmol/m^2 and 20.0 kJ/mol, 1.1 μmol/m^2 and 19.3 kJ/mol for TiO_2-{001}, TiO_2-{100}, TiO_2-{101} NCs, respectively. Thus, CH_4 adsorption on various TiO_2 NCs are similar, and the different adsorption amounts arise from both different density of adsorption sites and different coverages of carbonates, hydroxyl and water on various TiO_2 surfaces. The density of photoexcited electrons in the conduction band of various TiO_2 NCs upon UV light illumination was observed to decay much more slowly in CH_4 than in Ar (Figure 2a and Figure S16). Particularly, it remains unchanged for a long time for TiO_2-{001} NCs. Therefore, adsorbed CH_4 is capable of trapping photoexcited holes on the surfaces of various TiO_2 NCs, consequently prolonging the life of photoexcited electrons. The interfacial hole transfer from TiO_2 surface to adsorbed CH_4 is much more efficient on TiO_2-{001} NCs than on TiO_2-{100} and TiO_2-{101} NCs. Moreover, vibrational features of adsorbed formate species[45] appear on various TiO_2 NCs (Figure S17), confirming that adsorbed CH_4 undergoes photoexcited holes-mediated C-H bond activation reactions.

Photocatalytic CH_4 combustion over various TiO_2 NCs were studied using *in situ* DRIFTS spectra (Figure 3 a1-c1). Few feature of photoexcited electrons in the conduction band of TiO_2 could be observed due to their efficient scavenge by O_2 in the

reactants. Vibrational features of various surface intermediates, such as CH_3O (2941/2860 cm^{-1}), HCHO (1685 cm^{-1}), HCO (1708 cm^{-1}), HCOO (2953/2906/2870/2740/1552/1382/1358 cm^{-1}) and carbonates (1591/1309 cm^{-1})[30,44-48] were observed, resulting from the sequential photocatalytic oxidation reactions of CH_4 to CO_2. Temporal evolutions of observed intermediates on various TiO_2 NCs were plotted (Figure 3 a2-c2 and Figure S18-S20). The formate intermediate was observed to accumulate on all TiO_2 NCs, suggesting its photocatalytic oxidation as the rate-limiting step. On TiO_2-{001} NCs, the CH_3O intermediate accumulates on TiO_2-{001} NCs, demonstrating a faster CH_3O formation rate via CH_4 photooxidation than CH_3O photooxidation rate; the carbonates intermediates show almost unchanged coverage, indicating similar formation and consumption rates; and the HCHO and HCO intermediates were not observed, suggesting faster consumption rates than formation rates. On TiO_2-{100} NCs, few surface intermediates other than HCOO was observed, which, in combination with the photocatalytic activity, indicates a slow photooxidation rate of HCOO intermediate and faster photooxidation rates of CH_3O, HCHO and HCO intermediates than corresponding formation rates. On TiO_2-{101} NCs, the CH_3O intermediates show almost unchanged coverage, indicating similar formation and consumption rates; the HCHO and HCO intermediates initially emerge and then gradually disappears, suggesting faster photooxidation rates than corresponding formation rates; and the carbonates intermediates were barely observed, which, in combination with the photocatalytic activity, indicates a slow photooxidation rate. These results support that photocatalytic CH_4 activation and oxidation are more facile on TiO_2-{001} NCs than on TiO_2-{100} and TiO_2-{101} NCs.

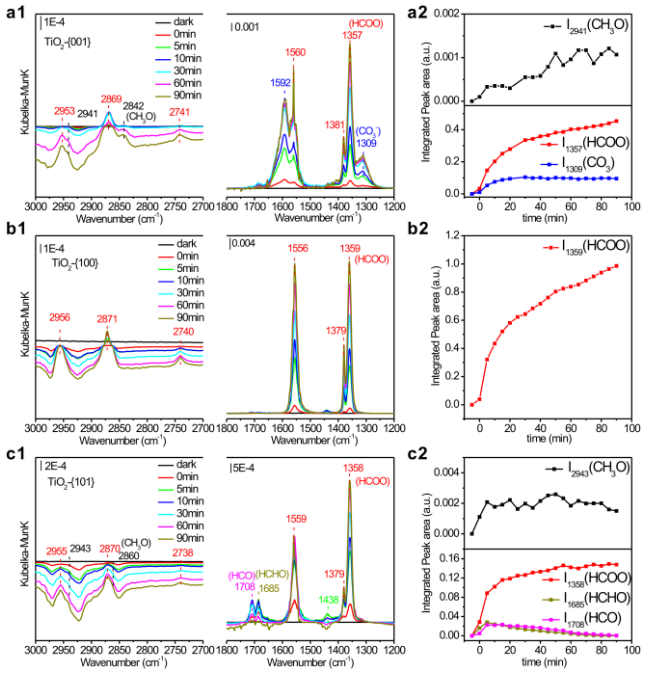

Figure 3. *In situ* and time-resolved DRIFTS spectra of photocatalytic methane oxidation and derived coverages of surface intermediates as a function of photocatalytic reaction time: (**a**) TiO_2-{001}, (**b**) TiO_2-{101} and (**c**) TiO_2-{100} NCs. DRIFTS spectra prior to UV light illumination were used as the background spectra.

DFT calculations were carried out to explore the CH_4/TiO_2 interfacial electronic structures which are critical for the interfacial charge transfer processes. The Ti cations and O anions in the bulk of anatase TiO_2 are sixfold-coordinated (Ti_{6c}) and threefold-coordinated (O_{3c}), respectively. As reported previously,[30,31,49-54] the anatase TiO_2(001) surface exhibits a typical reconstructed (001)-(1×4) surface exposing the reactive fourfold-coordinated Ti cations (Ti_{4c}) at the (1×4) added row, fivefold-coordinated Ti cations (Ti_{5c}) at the (1×1) basal surface and twofold-coordinated O anions at both the ridges ($O_{2c,r}$) and basal surface ($O_{2c,b}$), the anatase TiO_2(100) surface exhibits a typical reconstructed (1×2) surface exposing the Ti_{5c}, O_{2c} and $O_{3c,s}$ sites, and the anatase TiO_2(101) exhibits a (1×1) unreconstructed surface exposing the Ti_{5c}, O_{2c} and $O_{3c,s}$ sites. CH_4 adsorbs preferentially at the Ti_{4c} site of TiO_2(001)-(1×4) surface with an adsorption energy of -0.15 eV and at the Ti_{5c} site of TiO_2 (100) and (101) surfaces with adsorption energies respectively of -0.26 and -0.38 eV (Figure 4a1-a3). These calculation results suggest weak adsorption of CH_4 on various TiO_2 surfaces, consistent with the experimental results of adsorption microcalorimetry measurements. The valence and conduction bands of TiO_2 consist of the O 2p and Ti 3d orbitals, respectively. The calculated projected density of states (PDOS) results (Figure 4 b1-d1) interestingly reveal the presence of PDOS energy level differences of the Ti and O atoms between the TiO_2 bulk and TiO_2(001)-(1×4) surface but not between the TiO_2 bulk and TiO_2 (100) and (101) surfaces. The edge of the PDOS of bulk O_{3c} atoms is 0.49 eV lower than the edge of the PDOS of TiO_2(001)-(1×4) surface $O_{2c,r}$ atoms, while the edge of the PDOS of bulk Ti_{6c} atoms is 0.20 eV lower than the edge of the PDOS of TiO_2(001)-(1×4) surface Ti_{4c} atoms. This can be attributed to the very different surface structure of TiO_2(001)-(1×4) surface from those of TiO_2 (100) and (101) surfaces. Thus, the photoexcited electrons and holes within TiO_2 terminated with TiO_2(001)-(1×4) surface should occur spontaneous bulk-surface separation process to migrate to the bulk Ti_{6c} atoms and surface $O_{2c,r}$ atoms, respectively, whereas those within TiO_2 terminated with TiO_2 (100) and (101) surfaces should not. These results agree with the experimental results of NEXAFS and photoexcited charge density measurements. The PDOS energy levels of the Ti and O atoms in the bulk and on the surfaces remain unchanged upon CH_4 adsorption (Figure 4 b2-d2), but the CH_4/TiO_2 interfacial energy level alignments vary with the TiO_2 surfaces. The HOMO of CH_4 absorbed at the Ti_{4c} site of TiO_2(001)-(1×4) surface locates at the valence band maximum of TiO_2, whereas CH_4 absorbed at the Ti_{5c} site of TiO_2 (100) and (101) surfaces locates within the valence band of TiO_2. Therefore, CH_4 absorbed at the Ti_{4c} site of TiO_2(001)-(1×4) surface accepts the photoexcited holes in the valence band of TiO_2 more efficiently than CH_4 absorbed at the Ti_{5c} site of TiO_2 (100) and (101) surfaces, consistent with the experimental results of *in situ* DRIFTS measurements.

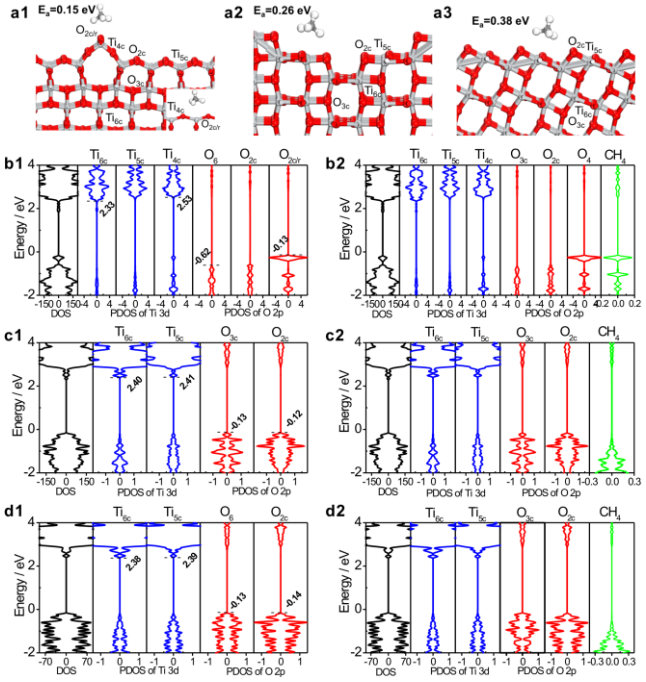

Figure 4. The most stable adsorption configurations of CH_4 on (**a1**) anatase TiO_2(001)-(1×4), (**a2**) anatase TiO_2(100)-(1×2) and (**a3**) anatase TiO_2(101) surfaces. Grey and red balls represent Ti and O atoms, respectively. Calculated DOS and PDOS of (**b1**) bare and (**b2**) CH_4-adsorbed anatase TiO_2(001)-(1×4) surfaces, (**c1**) bare and (**c2**) CH_4-adsorbed anatase TiO_2(100)-(1×2) surfaces, and (**d1**) bare and (**d2**) CH_4-adsorbed anatase TiO_2-(101) surfaces.

In summary, our combined experimental and theoretical calculation results demonstrate that surface structures of TiO_2 photocatalysts are capable of strongly affecting the bulk-surface charge separation processes and interfacial charge transfer processes at the CH_4/TiO_2 interfaces. TiO_2-{001} NCs terminated with the reconstructed (001)-(1×4) surface exhibit a spontaneous bulk-surface charge separation due to the locations of valence band maximum and conduction band minimum at the surface and in the bulk, respectively. Meanwhile, the HOMO of CH_4 adsorbed at the Ti_{4c} site of TiO_2(001)-(1×4) surface is localized at the valence band maximum. Therefore, TiO_2-{001} NCs show the photoexcited holes-enriched surface and efficient interfacial $TiO_2 \rightarrow CH_4$ hole transfer processes, leading to a high activity in photocatalytic methane combustion reaction. These results demonstrate surface structure engineering of semiconductor photocatalysts as an effective strategy to enhance photocatalytic efficiencies.

ASSOCIATED CONTENT

Supporting Information

Experimental and theoretical calculations details, XRD patterns, Transmission FTIR patterns and XPS spectra of various TiO_2 NCs and 1.24_{metal} wt.% Pt/TiO_2. Photoluminescence spectra of anatase TiO_2 and 1.24_{metal} wt.% Pt/TiO_2. The gas ratio of methane and oxygen on the rate of methane photocatalytic combustion in a flow-bed mode for TiO_2-{001} NCs and 1.24_{metal} wt.% Pt/TiO_2 samples. UV/Vis absorption spectra, Valence-band XP spectra and Photoluminescence spectra of various nanocrystals. ESR spectra of various NCs in the dark and under light irradiation. Time evolution of DRIFTS spectra in Ar/CH_4 atmosphere during UV irradiation for various nanocrystals. Ti L-edge and O K-edge NEXAFS spectra of TiO_2 NCs in the dark and under light irradiation. PES valence band spectra of various NCs in the dark and under light irradiation. DRIFTS spectra of methane absorption at dark condition. Adsorption-microcalorimetric results for various NCs. DRIFTS spectra with peak-fitting results of photocatalytic oxidation of methane on various NCs. This material is available free of charge via the Internet at http://pubs.acs.org.

AUTHOR INFORMATION

Corresponding Author

* E-mail address: huangwx@ustc.edu.cn (W.H.); xgong@ecust.edu.cn (X.Q.G.); junwang.tang@ucl.ac.uk (J.T.).

Author Contributions

‡These authors contributed equally.

Notes

The authors declare no competing financial interests.

ACKNOWLEDGMENT

This work was financially supported by the National Natural Science Foundation of China (21525313, 91745202, 92145302, 21773047, 21825301 and U1832180), the Chinese Academy of Sciences, the Changjiang Scholars Program of the Ministry of Education of China, and the University of Science and Technology of China (KY2060000176).

REFERENCES

(1) McFarland, E. Unconventional Chemistry for Unconventional Natural Gas. *Science* **2012**, *338*, 341-342.
(2) Brandt, A. R., Heath, G. A., Kort, E. A., O'Sullivan, F., Pétron, G., Jordaan, S. M., Tans, P., Wilcox, J., Gopstein, A. M., Arent, D., Wofsy, S., Brown, N. J., Bradley, R., Stucky, G. D., Eardley, D., Harriss, R. Methane Leaks from North American Natural Gas Systems. *Science* **2014**, *343*, 733-735.
(3) Nisbet, E. G.; Dlugokencky, E. J.; Bousquet, P. Methane on the Rise-Again. *Science* **2014**, *343*, 493-495.
(4) Lashof, D. A.; Ahuja, D. R. Relative Contributions of Greenhouse Gas Emissions to Global Warming. *Nature* **1990**, *344*, 529-531.
(5) Alvarez, R. A.; Pacala, S. W.; Winebrake, J. J.; Chameides, W. L.; Hamburg, S. P. Greater Focus Needed on Methane Leakage from Natural Gas Infrastructure. *Proc. Natl. Acad. Sci.* **2012**, *109*, 6435-6440.
(6) Cargnello, M.; Jaén, J. J. D.; Garrido, J. C. H.; Bakhmutsky, K.; Montini, T.; Gámez, J. J. C.; Gorte, R. J.; Fornasiero, P. Exceptional activity for methane combustion over modular $Pd@CeO_2$ subunits on functionalized Al_2O_3. *Science* **2012**, *337*, 713-717.
(7) Duan, H.; You, R.; Xu, S.; Li, Z.; Qian, K.; Cao, T.; Huang, W.; Bao, X. Pentacoordinated Al^{3+} -Stabilized Active Pd Structures on Al_2O_3 -Coated Palladium Catalysts for Methane Combustion. *Angew. Chem. Int. Ed.* **2019**, *58*, 12043-12048.
(8) Jiang, D.; Khivantsev, K.; Wang, Y. Low-Temperature Methane Oxidation for Efficient Emission Control in Natural Gas Vehicles: Pd and Beyond. *ACS Catal.* **2020**, *10*, 14304-14314.
(9) Song, H.; Meng, X.; Wang, Z.-j.; Liu, H.; Ye, J. Solar-Energy-Mediated Methane Conversion. *Joule* **2019**, *3*, 1606-1636.
(10) Li, Q.; Ouyang, Y.; Li, H.; Wang, L.; Zeng, J. Photocatalytic Conversion of Methane: Recent Advancements and Prospects. *Angew. Chem. Int. Ed.* **2021**, *60*, 2-29.
(11) Fujishima, A.; Zhang, X.; Tryk, D. TiO_2 Photocatalysis and Related Surface Phenomena. *Surf. Sci. Rep.* **2008**, *63*, 515-582.
(12) Chen, H.; Nanayakkara, C. E.; Grassian, V. H. Titanium Dioxide Photocatalysis in Atmospheric Chemistry. *Chem. Rev.* **2012**, *112*, 5919-5948.
(13) Chen, S.; Xiong, F.; Huang, W. Surface Chemistry and Catalysis of Oxide Model Catalysts from Single Crystals to Nanocrystals. *Surf. Sci. Rep.* **2019**, *74*, 100471.

(14) Wu, L.; Fu, C.; Huang, W. Surface Chemistry of TiO_2 Connecting Thermal Catalysis and Photocatalysis. *Phys. Chem. Chem. Phys.* **2020**, *22*, 9875-9909.
(15) Yang, H. G.; Sun, C. H.; Qiao, S. Z.; Zou, J.; Liu, G.; Smith, S. C.; Cheng, H. M.; Lu, G. Q. Anatase TiO_2 Single Crystals with a Large Percentage of Reactive Facets. *Nature* **2008**, *453*, 638-641.
(16) Fang, W. Q.; Gong, X.-Q.; Yang, H. G. On the Unusual Properties of Anatase TiO_2 Exposed by Highly Reactive Facets. *J. Phys. Chem. Lett.* **2011**, *2*, 725-734.
(17) Han, X.; Kuang, Q.; Jin, M.; Xie, Z.; Zheng, L. Synthesis of Titania Nanosheets with a High Percentage of Exposed (001) Facets and Related Photocatalytic Properties. *J. Am. Chem. Soc.* **2009**, *131*, 3152-3253.
(18) Xing, M.-Y.; Qi, D.-Y.; Zhang, J.-L.; Chen, F. One-Step Hydrothermal Method to Prepare Carbon and Lanthanum co-Doped TiO_2 Nanocrystals with Exposed {001} Facets and Their High UV and Visible-Light Photocatalytic Activity. *Chem. Eur. J.* **2011**, *17*, 11432-11436.
(19) Sun, L.; Zhao, Z.; Zhou, Y.; Liu, L. Anatase TiO_2 Nanocrystals with Exposed {001} Facets on Graphene Sheets Via Molecular Grafting for Enhanced Photocatalytic Activity. *Nanoscale* **2012**, *4*, 613-620.
(20) Ye, L.; Mao, J.; Liu, J.; Jiang, Z.; Peng, T.; Zan, L. Synthesis of Anatase TiO_2 Nanocrystals with {101}, {001} or {010} Single Facets of 90% Level Exposure and Liquid-Phase Photocatalytic Reduction and Oxidation Activity Orders. *J. Mater. Chem. A* **2013**, *1*, 10532-10537.
(21) Guo, Y.; Li, H.; Chen, J.; Wu, X.; Zhou, L. TiO_2 Mesocrystals Built of Nanocrystals with Exposed {001} Facets: Facile Synthesis and Superior Photocatalytic Ability. *J. Mater. Chem. A* **2014**, *2*, 19589-19593.
(22) Liu, Y.; Wang, M.; Li, D.; Fang, F.; Huang, W. Engineering Self-Doped Surface Defects of Anatase TiO_2 Nanosheets for Enhanced Photocatalytic Efficiency. *Appl. Surf. Sci.* **2021**, *540*, 148330.
(23) Pan, J.; Liu, G.; Lu, G. Q.; Cheng, H. M. On the True Photoreactivity Order of {001}, {010}, and {101} Facets of Anatase TiO_2 Crystals. *Angew. Chem. Int. Ed.* **2011**, *123*, 2181-2185.
(24) Gordon, T. R.; Cargnello, M.; Paik, T.; Mangolini, F.; Weber, R. T.; Fornasiero, P.; Murray, C. B. Nonaqueous Synthesis of TiO_2 Nanocrystals Using TiF_4 to Engineer Morphology, Oxygen Vacancy Concentration, and Photocatalytic Activity. *J. Am. Chem. Soc.* **2012**, *134*, 6751-61.
(25) Yu, J.; Low, J.; Xiao, W.; Zhou, P.; Jaroniec, M. Enhanced Photocatalytic CO_2-Reduction Activity of Anatase TiO_2 by Coexposed {001} and {101} Facets. *J. Am. Chem. Soc.* **2014**, *136*, 8839-8842.
(26) Tachikawa, T.; Wang, N.; Yamashita, S.; Cui, S. C.; Majima, T. Design of a Highly Sensitive Fluorescent Probe for Interfacial Electron Transfer on a TiO_2 Surface. *Angew. Chem. Int. Ed.* **2010**, *49*, 8593-8597.
(27) Tachikawa, T.; Yamashita, S.; Majima, T. Evidence for Crystal-Face-Dependent TiO_2 Photocatalysis from Single-Molecule Imaging and Kinetic Analysis. *J. Am. Chem. Soc.* **2011**, *133*, 7197-7204.
(28) D'Arienzo, M.; Carbajo, J.; Bahamonde, A.; Crippa, M.; Polizzi, S.; Scotti, R.; Wahba, L.; Morazzoni, F. Photogenerated Defects in Shape-Controlled TiO_2 Anatase Nanocrystals: A Probe to Evaluate the Role of Crystal Facets in Photocatalytic Processes. *J. Am. Chem. Soc.* **2011**, *133*, 17652-17661.
(29) Xiong, F.; Yin, L.-L.; Li, F.; Wu, Z.; Wang, Z.; Sun, G.; Xu, H.; Chai, P.; Gong, X.-Q.; Huang, W. Anatase TiO_2(001)-(1x4) Surface is Intrinsically More Photocatalytically Active Than Rutile TiO_2(110)-(1x1) Surface. *J. Phys. Chem. C* **2019**. *123*, 24558−24565.
(30) Fu, C.; Li, F.; Zhang, J.; Li, D.; Qian, K.; Liu, Y.; Tang, J.; Fan, F.; Zhang, Q.; Gong, X.; Huang, W. Site Sensitivity of Interfacial Charge Transfer and Photocatalytic Efficiency in Photocatalysis: Methanol Oxidation on Anatase TiO_2 Nanocrystals. *Angew. Chem. Int. Ed.* **2021**, *60*, 6160-6169.
(31) Xiong, F.; Yu, Y. Y.; Wu, Z.; Sun, G.; Ding, L.; Jin, Y.; Gong, X. Q.; Huang, W. Methanol Conversion into Dimethyl Ether on the Anatase TiO_2(001) Surface. *Angew. Chem. Int. Ed.* **2016**, *55*, 623-628.
(32) Lien, C.-F.; Chen, M.-T.; Lin, Y.-F.; Lin, J.-L. Photooxidation of Methane over TiO_2. *J. Chin. Chem. Soc.* **2004**, *51*, 37-42.
(33) Feng, N.; Lin, H.; Song, H.; Yang, L.; Tang, D.; Deng, F.; Ye, J. Efficient and Selective Photocatalytic CH_4 Conversion to CH_3OH with O_2 by Controlling Overoxidation on TiO_2. *Nat. Commun.* **2021**, *12*, 4652.
(34) Li, D.; You, R.; Yang, M.; Liu, Y.; Qian, K.; Chen, S.; Cao, T.; Zhang, Z.; Tian, J.; Huang, W. Morphology-Dependent Evolutions of Sizes, Structures, and Catalytic Activity of Au Nanoparticles on Anatase TiO_2 Nanocrystals. *J. Phys. Chem. C* **2019**, *123*, 10367-10376.
(35) Li, X.; Xie, J.; Rao, H.; Wang, C.; Tang, J. Platinum- and CuOx-Decorated TiO_2 Photocatalyst for Oxidative Coupling of Methane to C2 Hydrocarbons in a Flow Reactor. *Angew. Chem. Int. Ed.* **2020**, *59*, 19702-19707.
(36) Li, Z.; Boda, M. A.; Pan, X.; Yi, Z. Photocatalytic Oxidation of Small Molecular Hydrocarbons over ZnO Nanostructures: The Difference between Methane and Ethylene and the Impact of Polar and Nonpolar Facets. *ACS Sustainable Chem. Eng.* **2019**, *7*, 19042-19049.
(37) Li, Z.; Pan, X.; Yi, Z., Photocatalytic Oxidation of Methane over CuO-Decorated Zno Nanocatalysts. *J. Mater. Chem. A.* **2019**, *7*, 469-475.
(38) Chen, X.; Li, Y.; Pan, X.; Cortie, D.; Huang, X.; Yi, Z. J. Photocatalytic Oxidation of Methane over Silver Decorated Zinc Oxide Nanocatalysts. *Nat. Commun.* **2016**, *7*, 12273.
(39) Wei, J.; Yang, J.; Wen, Z.; Dai, J.; Li, Y.; Yao, B. Efficient Photocatalytic Oxidation of Methane over B-Ga_2O_3/Activated Carbon Composites. *RSC Adv.* **2017**, *7*, 37508-37521.
(40) Pan, X.; Chen, X.; Yi, Z. Photocatalytic Oxidation of Methane over $SrCO_3$ Decorated $SrTiO_3$ Nanocatalysts Via a Synergistic Effect. *Phys. Chem. Chem. Phys.* **2016**, *18*, 31400-31409.
(41) Berger, T.; Sterrer, M.; Diwald, O.; Knözinger, E.; Panayotov, D.; Thompson, T. L.; Yates, J. T. Light-Induced Charge Separation in Anatase TiO_2 Particles. *J. Phys. Chem. B* **2 2005**, *109*, 6061-6068.
(42) Wang, D.; Liu, L.; Sun, X.; Sham, T.-K. Observation of Lithiation-Induced Structural Variations in TiO_2 Nanotube Arrays by X-Ray Absorption Fine Structure. *J. Mater. Chem. A* **2015**, *3*, 412-419.
(43) Wendt, S.; Sprunger, P. T.; Lira, E.; Madsen, G. K.; Li, Z.; Hansen, J. Ø.; Matthiesen, J.; Blekinge-Rasmussen, A.; Lægsgaard, E.; Hammer, B. The Role of Interstitial Sites in the Ti3d Defect State in the Band Gap of Titania. *Science* **2008**, *320*, 1755-1759.
(44) Panayotov, D. A.; Burrows, S. P.; Morris, J. R. Photooxidation Mechanism of Methanol on Rutile TiO_2 Nanoparticles. *J. Phys. Chem. C* **2012**, *116*, 6623-6635.
(45) Wu, Y.; Gao, F.; Wang, H.; Kovarik, L.; Sudduth, B.; Wang, Y. Probing Acid–Base Properties of Anatase TiO_2 Nanoparticles with Dominant {001} and {101} Facets Using Methanol Chemisorption and Surface Reactions. *J. Phys. Chem. C* **2021**, *125*, 3988-4000.
(46) Chen, X.; He, G.; Li, Y.; Chen, M.; Qin, X.; Zhang, C.; He, H. Identification of a Facile Pathway for Dioxymethylene Conversion to Formate Catalyzed by Surface Hydroxyl on TiO_2-Based Catalyst. *ACS Catal.* **2020**, *10*, 9706-9715.
(47) Liao, L.-F.; Wu, W.-C.; Chen, C.-Y.; Lin, J.-L. Photooxidation of Formic Acid Vs Formate and Ethanol vs Ethoxy on TiO_2 and Effect of Adsorbed Water on the Rates of Formate and Formic Acid Photooxidation. *J. Phys. Chem. B* **2001**, *105*, 7678-7685.
(48) Chen, S.; Cao, T.; Gao, Y.; Li, D.; Xiong, F.; Huang, W. Probing Surface Structures of CeO_2, TiO_2, and Cu_2O Nanocrystals with CO and CO_2 Chemisorption. *J. Phys. Chem. C* **2016**, *120*, 21472-21485.
(49) Li, Y., et al., Wu, X. P., Jiang, N., Lin, M., Shen, L., Sun, H., Wang, Y., Wang, M., Ke, X., Yu, Z., Gao, F., Dong, L., Guo, X., Hou, W., Ding, W., Gong, X., Grey, C. P., Peng, L. Distinguishing Faceted Oxide Nanocrystals with ^{17}O Solid-State NMR Spectroscopy. *Nat. Commun.* **2017**, *8*, 581.
(50) Yuan, W.; Wang, Y.; Li, H.; Wu, H.; Zhang, Z.; Selloni, A.; Sun, C. Real-Time Observation of Reconstruction Dynamics on TiO_2(001) Surface under Oxygen Via an Environmental Transmission Electron Microscope. *Nano Lett.* **2016**, *16*, 132-137.
(51) Beinik, I.; Bruix, A.; Li, Z.; Adamsen, K. C.; Koust, S.; Hammer, B.; Wendt, S.; Lauritsen, J. V. Water Dissociation and Hydroxyl Ordering on Anatase TiO_2(001)-(1×4). *Phys. Rev. Lett.* **2018**, *121*, 206003.

(52) Ruzycki, N.; Herman, G. S.; Boatner, L. A.; Diebold, U. Scanning Tunneling Microscopy Study of the Anatase (100) Surface. *Surf. Sci. Lett.* **2003**, *529*, 239-244.
(53) Zuleta, M.; Yu, S.; Ahmadi, S.; Boschloo, G.; Go¨thelid, M.; Hagfeldt, A. Monitoring N719 Dye Configurations on (1×N)-Reconstructed Anatase (100) by Means of STM: Reversible Configurational Changes Upon Illumination. *Langmuir* **2010**, *26*, 13236-13244.
(54) Hebenstreit, W.; Ruzycki, N.; Herman, G. S.; Gao, Y.; Diebold, U. Scanning Tunneling Microscopy Investigation of the TiO_2 Anatase (101) Surface. *Phys. Rev. B* **2000**, *62*, R16334.

SYNOPSIS TOC